JCTC Journal of Chemical Theory and Computation

Performance of the Density Functional Theory/ Multireference Configuration Interaction Method on Electronic Excitation of Extended π-Systems

Christel M. Marian* and Natalie Gilka†

Institute of Theoretical and Computational Chemistry, Heinrich-Heine-University Düsseldorf, Universitätsstraβe 1, 40225 Düsseldorf, Germany

Received May 19, 2008

Abstract: The combined density functional theory/multireference configuration interaction (DFT/MRCI) method [Grimme and Waletzke. *J. Chem. Phys.* 1999, *111*, 5645] has been employed to study the ^1L_a and ^1L_b states of linear polyacenes and the low-lying triplet and singlet states of linear polyenes and diphenyl-polyenes. We have systematically investigated the dependence of the electronic state properties on technical parameters of the calculations such as the atomic orbital basis set or the geometry optimization approach. The choice of basis set appears to be of minor importance whereas the excitation energies of the polyenes are quite sensitive to the ground-state geometry parameters. The DFT/MRCI energies at the B3-LYP optimized geometries systematically underestimate the experimental values, but we do not observe a bias toward one or the other type of state. The energy gaps between the electronically excited states are reproduced very well. In particular, this applies also to the first excited singlet $2\,^1A_g^-$ and the optically bright $^1B_u^+$ state of the polyenes. The latter appears to be the S_3 or even S_4 state in longer polyenes where the multiconfigurational $^1B_u^-$ state represents S_2. Frequencies and intensities of the excited-state absorption from the $2\,^1A_g^-$ state are found to be strongly geometry dependent.

1. Introduction

Many biologically relevant pigments such as carotenoids and retinal contain extended polyene chromophores. Naturally occurring carotenoids possess between 7 and 11 conjugated double bonds and exhibit a variety of low-lying electronic states, many of which are not easily accessed spectroscopically because the corresponding one-photon transition from the ground state is forbidden (*gerade*-states, triplets, double excitations).[1] A reliable quantum chemical description of these states could therefore help understanding the intricate photophysical relaxation mechanisms these molecules undergo after electronic excitation.

In recent years, time-dependent density functional theory (TDDFT) has emerged as standard tool for the evaluation of electronically excited states of large molecules for which traditional wave function based methods are not feasible. Unfortunately, TDDFT in combination with standard functionals fails in describing the correct ordering of the two lowest excited singlet states of linear polyenes and carotenoids.[2−5] The Tamm−Dancoff approximation (TDA) to TDDFT appears to perform better in this respect.[2] However, the success of this method was recently shown to be based on fortuitous cancelation of errors.[6] It has been firmly established that the optically bright ^1B_u state which originates from the (HOMO → LUMO) single excitation is not the lowest excited singlet state in linear polyenes, possibly except for butadiene.[7,8] Instead, the S_1 state possesses ^1A_g symmetry and exhibits a highly multiconfigurational character with the (HOMO → LUMO)^2, (HOMO − 1 → LUMO), and (HOMO → LUMO + 1) configurations as leading terms.[9−11] Complete active space second-order perturbation theory (CASPT2)

* To whom correspondence should be addressed. Tel.: +49-211-8113209. Fax: +49-211-8113446. E-mail: Christel.Marian@uni-duesseldorf.de.

† Present address: Department of Chemistry, University of Warwick, CV4 7AL, Coventry, UK.

10.1021/ct8001738 CCC: $40.75
Published on Web 08/15/2008

or more general multireference second-order perturbation theory (MRMP2) treatments of the electron correlation are capable of describing these states and their energetic ordering properly.[12−14] With increasing chain length it becomes more and more demanding, however, to include the appropriate orbitals in the active space. To the best of the authors' knowledge, no CASPT2 or MRMP2 treatment has been published for polyenes with seven or more conjugated double bonds. Coupled-cluster calculations with single and double excitations (albeit with an approximate treatment of the doubles, CC2) can in principle be applied to study the electronically excited states of large molecules. However, because of the double-excitation character of the $2\ ^1A_g$ state, also this method places the $2\ ^1A_g$ state considerably above the $1\ ^1B_u$ state in hexatriene[15−17] and octatetraene.[17] The second-order algebraic diagrammatic construction (ADC(2)) method[18] allows in principle for the consistent treatment of doubly excited states. Applications to several polyenes including a treatment of doubly excited configurations through zeroth (ADC(2)-s) or first order (ADC(2)-x) are available[6] and will be discussed below.

Another spectroscopically important class of molecules with extended π-systems are linear condensed acenes. Parac and Grimme[19] could show that TDDFT yields substantial errors in the description of the short-axis polarized L_a state while the long-axis polarized L_b is described well. The CC2 method, on the other hand, achieves a balanced description of the two states, in this case. Here, the difficulties do not arise from a double excitation character as for the $2\ ^1A_g$ state of the polyenes. For benzene they were shown to result from large dynamical $\sigma-\pi$ polarization effects.[20]

In the present work, we investigate the performance of the combined density functional theory and multireference configuration interaction method (DFT/MRCI)[21] on low-lying singlet and triplet states of polyenes, α,ω-diphenyl-polyenes, and polyacenes. The DFT/MRCI method has been shown to yield reliable excitation energies and transition moments at reasonable cost for a variety of molecules.[17,21−27] Particular emphasis is put on the above-mentioned critical cases, namely the $2\ ^1A_g$ and $1\ ^1B_u$ states of polyenes and α,ω-diphenyl-polyenes as well as the L_a and L_b states of polyacenes. In addition, we study trends of the properties of further low-lying states in the series of *all-trans*-polyenes beginning with 1,3,5-hexatriene and extending to 1,3,5,7,9,11,13,15,17,19,21,23,25-hexacosatridecaene, as the location of these states may be important for the excited-state absorption (ESA) and for the relaxation dynamics following the population of the optically bright (HOMO → LUMO) singlet excited state.

2. Methods and Technical Details

Computations on larger polyenes may become cumbersome if extended basis sets are used. Therefore, our first issue was a search for technical parameters of the calculation with optimal cost/performance ratio.

Three qualitatively different basis sets from the Turbomole library[28] were employed: the split valence basis set with (d) polarization functions for non-hydrogen atoms, (SV(P)), the valence triple-ζ basis set with polarization functions (d,p) (TZVP), and the valence triple-ζ basis set with a double set of polarization functions (2d1f,2p1d) (TZVPP). If not specified otherwise, the equilibrium nuclear arrangements of the electronic ground states were determined using density functional theory (DFT) in combination with a restricted closed-shell Kohn−Sham determinant. The geometries of the first excited triplet states were optimized utilizing unrestricted DFT (UDFT). Finally, TDDFT[29] was used to obtain the minimum geometries of the singlet-coupled (HOMO → LUMO) excited states. These calculations were carried out employing the Turbomole suite of programs.[30] We also tested the performance of different density functionals for geometry optimization. Among these, the local B-LYP functional[31,32] is the less expensive one in terms of computer time because one can make use of the resolution-of-the-identity (RI) approximation.[33,34] The second functional used is the well-known B3-LYP functional.[32,35,36] It typically yields reliable bond distances and frequencies. Since it is a hybrid functional which includes 20% Hartree−Fock exchange, no use of the RI approximation can be made. The third functional, BH-LYP,[32,37] includes 50% Hartree−Fock exchange. In combination with the DFT/MRCI approach it is the standard functional used for generating the MO basis and Fock matrix elements. With regard to minimum geometries it is known to yield typically somewhat too compact molecular structures. As purely wave function based methods Hartree−Fock (HF) and second-order Møller−Plesset perturbation theory (MP2) are employed in a few test cases.

Electronic excitation energies are evaluated by means of the DFT/MRCI method.[21] The idea behind this approach is to include major parts of dynamic electron correlation by density functional theory whereas short to medium-sized MRCI expansions take account of static correlation effects. In this way, severe size-extensivity problems can be avoided even for systems with many valence electrons. The configurations in the MRCI expansion are built up from Kohn−Sham (KS) orbitals of a closed-shell reference state. In the effective DFT/MRCI Hamiltonian, five empirical parameters (scaling factors for Coulomb and exchange integrals as well as energy cutoff parameters) are employed that depend only on the multiplicity of the desired state, the number of open shells of a configuration, and the type of density functional employed, but not on the specific atom or molecule. To avoid double-counting of dynamic correlation, the MRCI expansion is kept short by extensive configuration selection. Currently, optimized parameter sets for the effective DFT/MRCI Hamiltonian are available in combination with the BH-LYP functional. We employ the original set of parameters[21] here in combination with an orbital selection threshold of $1.0E_H$. For details concerning the integration of DFT information into the MRCI procedure and the parameter fitting, we refer to the original publications.[21]

3. Results and Discussion

3.1. Benchmark Systems. *3.1.1. Linear Conjugated Acenes.* TDDFT in combination with standard functionals has been shown to give dramatic failures for the short-axis polarized ^1L_a state of linear conjugated acenes.[19] The ^1L_a

Table 1. Calculated Vertical Absorption Energies ΔE_{vert} [eV] of Linear Condensed Acenes in Comparison with Previous Theoretical Results and Experimental Values[a]

number of rings	DFT/MRCI SV(P)	DFT/MRCI TZVP	BP86[b]	B3-LYP[c]	CC2[d]	exp[e]
			1 $^1B_{2u}$, ^1L_a state			
2	4.70 (0.1257)	4.66 (0.1222)	4.11	4.38	4.88	4.66
3	3.53 (0.1279)	3.51 (0.1249)	2.95	3.21	3.69	3.60
4	2.75 (0.1111)	2.74 (0.1088)	2.17	2.43	2.90	2.88
5	2.22 (0.0929)	2.22 (0.0916)	1.63	1.89	2.35	2.37
6	1.86 (0.0749)	1.85 (0.0744)	1.23	1.49	1.95	2.02
8	1.46 (0.0407)	1.44 (0.0418)	0.68	0.94	1.43	1.58
			1 $^1B_{3u}$, ^1L_b state			
2	4.13 (0.0002)	4.15 (0.0001)	4.13	4.26	4.47	4.46
3	3.56 (0.0012)	3.59 (0.0007)	3.64	3.87	3.89	3.64
4	3.20 (0.0034)	3.22 (0.0023)	3.24	3.47	3.52	3.39
5	2.96 (0.0069)	2.99 (0.0054)	2.96	3.21	3.27	3.12
6[f]	2.72 (0.0051)	2.76 (0.0051)	2.76	3.02	3.09	2.87
	2.90 (0.0066)	2.93 (0.0045)				
8	2.77 (0.0269)	2.78 (0.0244)	2.50	2.77	2.87	

[a] Oscillator strengths $f(r)$ are given in parentheses. [b] See ref 19 for TDDFT(BP86) using Dunning's cc-pVTZ basis at the ground-state geometry obtained from DFT(B3-LYP) calculations in a TZVP basis. [c] See ref 19 for TDDFT(B3-LYP) using Dunning's cc-pVTZ basis at the ground-state geometry obtained from DFT(B3-LYP) calculations in a TZVP basis. [d] See ref 19 for CC2 using Dunning's cc-pVTZ basis at the ground-state geometry obtained from DFT(B3-LYP) calculations in a TZVP basis. [e] Derived from 0−0 transition energies in solution.[38] For details see ref 19. [f] The (HOMO − 2 → LUMO) and (HOMO → LUMO + 2) configurations are spread over the 1 $^1B_{3u}$ and 2 $^1B_{3u}$ DFT/MRCI wave functions. Due to their energetic proximity and mixed wave function character, the two low-lying $^1B_{3u}$ states exhibit similar oscillator strengths and together make up the ^1L_b state in this molecule. For this reason, two values are listed.

state has $^1B_{2u}$ symmetry and results from the (HOMO → LUMO) excitation. In a valence-bond picture, this state exhibits large contributions from ionic components. In addition to the ^1L_a state, Parac and Grimme[19] studied the long-axis polarized ^1L_b state. The latter state exhibits $^1B_{3u}$ symmetry. Its electronic structure is mainly covalent. For molecules with 2−4 conjugated rings, its wave function is dominated by a nearly equal mixture of (HOMO − 1 → LUMO) and (HOMO → LUMO + 1) excitations.

We computed vertical DFT/MRCI excitation energies at DFT(B3-LYP) optimized geometries for polyacenes with 2−6 and with 8 rings using both SV(P) and TZVP basis sets. Our results are collected in Table 1 and are compared to the TDDFT and CC2 excitation energies of Parac and Grimme.[19] These authors also published estimates of vertical experimental excitation energies which they derived from experimental 0−0 data[38] by correcting for solvent and relaxation effects. These estimates are displayed in Table 1 as well. It is seen that the DFT/MRCI results do not suffer from the flaws of the TDDFT treatments. Actually, their accuracy is comparable to the one of the ab initio CC2 method, but with a tendency of slightly underestimating the ^1L_a and ^1L_b excitation energies whereas CC2 overestimates the experimental values by approximately the same amount. With regard to the treatment of large π-systems, it is encouraging that the reduction of the basis set quality from TZVP to SV(P) has almost no effect on the DFT/MRCI excitation energies. The underlying reason for this behavior is the fact that the (virtual) DFT orbitals are significantly less diffuse than HF orbitals. Thus, the basis set size does not influence the orbital energies as much as in HF.

Before we take a more detailed look at the ^1L_b and ^1L_a energies, a short overview over the energetic order of molecular orbitals will be given. In the compounds with even number of rings, the HOMO − 1 belongs to the b_{1u} irreducible representation (irrep) of the D_{2h} molecular point group, the HOMO has a_u symmetry, while the virtual orbitals LUMO and LUMO + 1 transform according to the b_{2g} and b_{3g} irreps, respectively. In anthracene, the order is reversed with b_{2g} and b_{3g} orbitals building HOMO − 1 and HOMO, respectively, and LUMO and LUMO + 1 belonging to the b_{1u} and a_u irreps, respectively. According to our calculations, the order of the frontier orbitals becomes irregular for the polyacenes with more than 4 rings. While the identity of HOMO and LUMO is preserved, we find the highest occupied b_{2g} orbital as HOMO − 2 in pentacene, with an orbital of a_u symmetry forming HOMO − 1. A similar situation is found for the unoccupied orbitals. Here, an orbital of b_{2g} symmetry forms the LUMO + 1 while the lowest unoccupied orbital of a_u symmetry is LUMO + 2. Accordingly, we find the (HOMO − 2 → LUMO) and (HOMO → LUMO + 2) excitations to be dominating the electronic structure of the ^1L_b state. Similarly, the highest occupied b_{1u} orbital has been shifted to HOMO − 2 in hexacene and the lowest unoccupied b_{3g} orbital is LUMO + 2 here. HOMO − 1 exhibits b_{3g} symmetry while the LUMO + 1 belongs to the b_{1u} irrep. The tendency of shifting the orbitals, involved in the ^1L_b excitation, away from the Fermi level continues in octacene. Here, the corresponding b_{1u} and b_{3g} orbitals yield HOMO − 3 and LUMO + 3, respectively.

A close look at the excitation energies of particular members of this series in Table 1 shows that the DFT/MRCI and CC2 methods correctly predict the swap of energetic order of the ^1L_b and ^1L_a states to occur between $n = 2$ and $n = 3$. In polyacenes with 3−6 conjugated rings, the ^1L_a state represents the S_1 state. In octacene, our DFT/MRCI calculation yields 2 ^1A_g as the first excited singlet state. Its MRCI expansion is dominated by double excitations with the leading term being the (HOMO → LUMO)^2 configuration. In contrast to the situation in linear polyenes (see below)

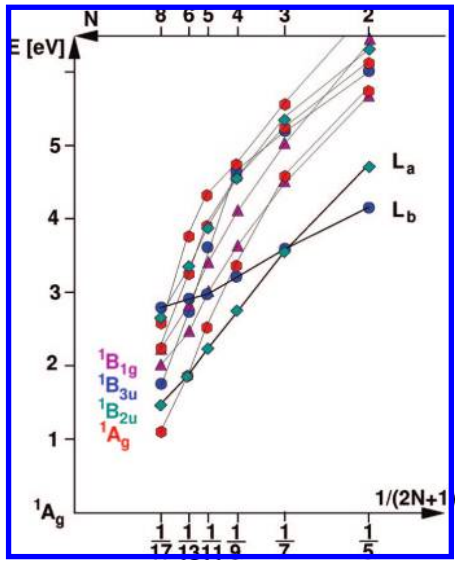

Figure 1. DFT/MRCI vertical electronic excitation energies of polyacenes at the respective 1 ^1A_g ground-state minimum geometry as functions of the number of condensed rings *N*. Hexagons symbolize ^1A_g, diamonds $^1B_{2u}$, circles $^1B_{3u}$, and triangles $^1B_{1g}$.

its wave function has very little contributions from single excitations. The 1 $^1A_g \rightarrow 2\ ^1A_g$ one-photon transition is symmetry-forbidden so that we do not expect to see this state in the absorption spectrum of octacene. The ^1L_a state represents the S_2 state here.

The excitation energy of the ^1L_b state varies significantly less than the one of the ^1L_a and other low-lying singlet states. With extending molecular size, the ^1L_b state therefore switches order quite often (Figure 1). It represents the S_1 state in naphthalene, shifts to S_2 in anthracene and tetracene, and is the third excited singlet (S_3) in pentacene where the doubly excited 2 ^1A_g state takes the position of the S_2 state. As mentioned above, the leading configurations of the 1 $^1B_{3u}$ (^1L_b) state are (HOMO − 2 → LUMO) and (HOMO → LUMO + 2) here. The 1 $^1B_{1g}$ state lies very close by (at 2.99 eV in the SV(P) basis and at 3.02 in the TZVP basis) but is optically dark. Its wave function has large contributions from (HOMO − 1 → LUMO), (HOMO → LUMO + 1), and double excitations. The situation is even more complex in hexacene. As in pentacene, the S_2 state is the doubly excited 2 ^1A_g. The 1 $^1B_{1g}$ has dropped below the ^1L_b state and forms S_3. The 1 $^1B_{3u}$ state is the fourth excited singlet in hexacene. Unlike the situation in the smaller polyacenes, its wave function is dominated by the double excitations (HOMO − 1, HOMO → LUMO^2) and (HOMO^2 → LUMO, LUMO + 1), but has still large components from (HOMO − 2 → LUMO) and (HOMO → LUMO + 2). The latter are the leading configurations in 2 $^1B_{3u}$ which corresponds to S_6 in this molecule. Due to their energetic proximity and mixed wave function character, the two low-lying $^1B_{3u}$ states exhibit similar oscillator strengths and together make up the ^1L_b state. For this reason, two values are listed as ^1L_b excitation energy in Table 1. In octacene, the near-degeneracy of the 1 $^1B_{3u}$ and 2 $^1B_{3u}$ states does not persist. Although the 1 $^1A_g \rightarrow 1\ ^1B_{3u}$ transition at 1.46 eV (SV(P) basis) is formally symmetry-allowed, it is one-photon forbidden because of the double-excitation character of the state. The 2 $^1B_{3u}$ (S_9) wave function clearly represents the ^1L_b state in octacene, closely followed by another optically allowed transition, 1 $^1A_g \rightarrow 3\ ^1B_{2u}$, at 2.86 eV (SV(P) basis).

3.1.2. Short Linear Polyenes. For the first members of the series, gas phase spectra or high-resolution spectra of jet-cooled molecules are available.[39−47] These experimental conditions guarantee that environmental effects on the spectra are small. Electron impact studies[48−51] revealed the approximate positions of triplet states. Furthermore, bond lengths of *trans*-1,3,5-hexatriene have been determined experimentally by gas phase electron diffraction.[52] In addition, low-temperature spectra of short polyenes have been recorded with high resolution in Shpolskii matrices of *n*-alkanes.[53−55] Comparison of the band positions with gas phase spectra can thus provide an estimate of solvent shifts. In addition to numerous experimental investigations, extensive theoretical studies with ab initio wave function methods,[12−14,16,17,56−62] and (TD)DFT[2−4,15,63] have been carried out.

For these reasons, we have chosen *trans*-1,3,5-hexatriene (HT), *trans*,*trans*-1,3,5,7-octatetraene (OT), and *all-trans*-1,3,5,7,9-decapentaene (DP) as benchmark systems for which detailed comparison with experimental data is made. Moreover, these molecules are small enough to test basis set effects on the geometrical parameters and on the spectral properties.

Hexatriene. Conflicting results exist on the energetic position of the 2 ^1A_g state of HT. Buma et al.[44] and Petek et al.[45] have shown by means of fluorescence excitation spectroscopy that a one-photon forbidden state with origin at 4.26 eV (presumably 2 $^1A_1$) lies below the optically allowed 1 $^1B_2$ state in isolated *cis*-hexatriene. The origin of the corresponding 2 ^1A_g of *trans*-hexatriene has not been observed, but it can be assumed to lie within a few hundred wavenumbers of the *cis*-band. Coherent anti-Stokes Raman scattering (CARS) and coherent Stokes Raman scattering (CSRS) experiments on liquid *cis*- and *trans*-hexatriene were carried out at ambient temperatures by Fujii et al.[64] These authors report the two-photon absorption (TPA) band to lie a few thousand inverse centimeters above the intense dipole-allowed one-photon transitions (1 $^1B_2 \leftarrow 1\ ^1A_1$ (cis) or 1 $^1B_u \leftarrow 1\ ^1A_g$ (trans)). In light of the results of Buma et al.[44] and Petek et al.,[45] the assignment of this TPA band to the 2 $^1A_1 \leftarrow 1\ ^1A_1$ or 1 $^1B_u \leftarrow 1\ ^1A_g$ appears questionable at first sight. As we shall see below, our calculations can help to resolve this conflict. The position of the 1 $^1B_u \leftarrow 1\ ^1A_g$ origin is unambiguous, on the other hand. The origin peak—which is also the strongest peak in the spectrum—is reported at 4.93 eV in gas phase absorption spectra[42,65] and at 4.95 eV in a resonant enhanced multiphoton ionization (REMPI) spectrum.[46] The strong origin transition of the 1 $^1B_u \leftarrow 1\ ^1A_g$ band and the lack of extended vibrational structure led Leopold et al.[42] to the conclusion that the geometry of the 1 ^1B_u state is not largely distorted, i.e., in particular it is believed to be planar. Myers and Pranata[66] come to a similar conclusion with regard to planarity but report significant reductions in the force constants for both terminal and central double-bond twisting with respect to the ground state.

Table 2. Basis Set Dependence of Vertical DFT/MRCI Absorption Energies ΔE_{vert} [eV] of HT in Comparison with Previous Theoretical Results of Correlated ab initio Wave Function Methods and Experimental Values

method	DFT/MRCI			QCI/CI6[a]	CASPT2[b,c,d]			CC2[d]	CCSD[d]	CC3[d]	ADC(2)-s[e]	ADC(2)-x[e]	
basis	SV(P)	TZVP	TZVPP										λ_{max}
$2\,^1A_g$	4.95	4.96	4.98	5.74	5.19	5.34	5.42	6.67	6.61	5.72	6.75	4.07	5.21[f]
$1\,^1B_u$	5.07	4.97	4.94	5.14	5.01	5.37	5.31	5.41	5.72	5.58	5.36	5.15	5.13[g], 4.93[h,i]
$1\,^3B_u$	2.46	2.47	2.49	2.84	2.55	2.60	2.71	2.78	2.62	2.69			2.61[g]
$1\,^3A_g$	4.01	3.99	4.01		4.12	4.24	4.31	4.40	4.28	4.32			4.11[g]

[a] See ref 56. QCI for $2\,^1A_g$, CI6 + SC for $1\,^1B_u$ and $1\,^3B_u$. [b] See ref 12. CASPT2 based on CASSCF with 6 active electrons in 4 a_u and 4 b_g active orbitals, (6s3p1d/2s1p) ANO basis + Rydberg functions, and experimental geometry parameters. [c] See ref 14. CASPT2 based on CASSCF with 6 active electrons in 12 active orbitals, (3s2p1d/2s) basis, and experimental geometry parameters. [d] See ref 17. CASPT2 based on CASSCF with 6 active electrons in 6 active orbitals, TZVP basis, and ground-state MP2/6-31G* geometry. [e] See ref 6. TZVP basis and ground-state MP2/6-31G* geometry. [f] See ref 64. TPA maxiumum of liquid HT at room temperature. [g] See ref 49. Band maximum of low-energy electron impact spectrum. [h] See ref 42. 0−0 transition and absorption maximum of jet-cooled HT. [i] See ref 39. 0−0 transition and absorption maximum of isolated HT.

Electron impact studies[48,49] observe a different intensity distribution of the transition. Flicker et al.[49] find the 0−0 transition at 4.95 eV in agreement with optical spectra but the band maximum occurs at 5.13 eV. Despite considerable effort no emission has been observed from *trans*-1,3,5-hexatriene after $1\,^1B_u \leftarrow 1\,^1A_g$ excitation. According to Leopold et al.,[42] the observed broadband widths of the hexatriene absorption spectrum appear to be compatible with an extremely short lifetime of the primarily excited state due to ultrafast internal conversion to a lower-lying singlet. Transitions to higher-lying singlet states of HT were observed by Gavin and Rice[39] but were assigned to Rydberg transitions. Since we did not include diffuse basis functions, a comparison with experiment cannot be made in these cases.

Due to different selection rules, transitions to triplet states can be observed with high intensity by means of electron impact spectroscopy. Vertical excitation energies were published for T_1 (2.61 eV, $1\,^3B_u$) and T_2 (4.11 eV, $1\,^3A_g$).[49] Frueholz and Kuppermann[50] could resolve the vibronic structure of the second triplet and were thus able to determine its adiabatic excitation energy (3.75 eV).

The vertical DFT/MRCI excitation energies of HT (Table 2) show a similar trend as already observed for the polyacenes. For the two lowest singlet states, the experimental reference values are underestimated by about 0.2 eV, but no preference is given to either the $2\,^1A_g$ or the $1\,^1B_u$ state. Both are found to be nearly degenerate in the Franck−Condon (FC) region, in agreement with CASPT2 results[12,14,17] and experimental evidence.[42] In contrast, the coupled-cluster methods with single and double excitation operators (CCSD and CC2)[17] and the strict ADC(2) approach, ADC(2)-s,[6] yield very large energy gaps. It appears that they do not properly account for the multiconfiguration effects in the $2\,^1A_g$ state. In HT, the (HOMO − 1 → LUMO) and (HOMO → LUMO + 1) single excitations are prominent configurations in the CI expansion of the S_1 state, but unlike the situation in short polyacenes, they are not the leading terms. The latter is dominated by the (HOMO → LUMO)^2 double excitation instead. The extended ADC(2) method, ADC(2)-x, which includes the treatment of double excitations through first order, seems to overshoot, yielding a significantly too low excitation energy of the $2\,^1A_g$ state in HT.[6] With regard to the basis set dependence of the DFT/MRCI results, only slight variations of the $2\,^1A_g$ excitation energy are observed. The $1\,^1B_u$ state, which originates from the (HOMO → LUMO) excitation and corresponds to ionic valence-bond structures, appears to be more sensitive to the quality of the basis set. The two lowest triplet states are mainly represented by single excitations. As observed already by Schreiber et al.[17] their correlation treatment is less demanding. Here, all the methods perform equally well.

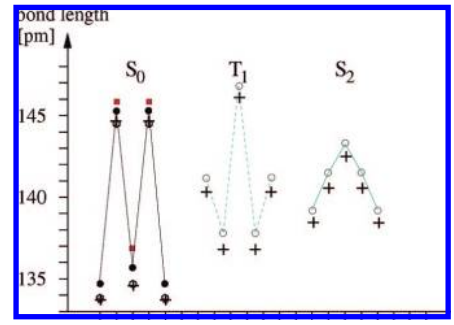

Figure 2. C−C bond lengths of *trans*-1,3,5-hexatriene in the $1\,^1A_g$ electronic ground state (left), the first excited triplet state $1\,^3B_u$ (middle), and the optically bright $1\,^1B_u$ state (right). Calculated values are represented by circles (B3-LYP, SV(P) basis), plus signs (B3-LYP, TZVP basis), and hexagons (B3-LYP, TZVPP basis). Squares correspond to experimentally derived values determined from gas phase electron diffraction.[52]

In order to distinguish direct basis set effects on the excitation energy and indirect effects through the geometry, we carried out single-point DFT/MRCI calculations in the SV(P) basis set at the ground-state geometries obtained from B3-LYP optimizations in the TZVP and TZVPP bases, respectively, for the wave function methods HF, RIMP2, and MP2 and for a structure with experimentally derived bond distances.[52] The TZVP- and TZVPP-optimized geometries are practically identical while the bond distances of the SV(P)-optimized structure are consistently longer by about 1 pm (see Figure 2). Comparison to the geometry parameters derived from the X-ray structure of gaseous HT[52] shows that the terminal double bond length is reproduced excellently in the calculations using at least a TZVP basis. Our value for the central double bond distance (134.7 pm) is in good agreement with the CASSCF value of 134.5 pm by Nakayama et al.[14] but is markedly shorter than the experimental value (136.7 pm).[52] We refrained from optimizing the geometry of the $2\,^1A_g$ state because of its double excitation character. For the T_1 state ($1\,^3B_u$), a reversal of single and

Table 3. Calculated Adiabatic DFT/MRCI Excitation Energies ΔE_{adia} [eV] of HT in Comparison with Experimental Values

	ΔE_{adia} (DFT/MRCI)		
state	SV(P)	TZVP	ΔE_{0-0}
$2\,^1A_g$	4.07[a]	4.08[a]	4.26[b]
$1\,^1B_u$	4.79	4.67	4.93[c, d], 4.94[e], 4.95[f]
$1\,^3B_u$	1.90	1.94	

[a] Energy at the $1\,^3B_u$ minimum. [b] See ref 45. Fluorescence excitation of jet-cooled *cis*-1,3,5-hexatriene. [c] See ref 65. Absorption of isolated HT. [d] See ref 42. Absorption of jet-cooled HT. [e] See ref 46. REMPI spectrum. [f] See ref 49. Low-energy electron impact.

double bond character is found with the difference between double and single bond being less pronounced than in the ground state. The bond length alternation is even smaller in the $1\,^1B_u$ state. In both cases, the trends for the SV(P) and TZVP bases are the same as for the ground state, i.e., the SV(P) basis yields minimum nuclear structures with slightly longer bonds. Detailed results of the single-point calculations are available in the Supporting Information (SI). In all cases, the DFT/MRCI excitation energy obtained with the SV(P) basis at the SV(P)-optimized geometry agrees much better with the TZVP and TZVPP results than the DFT/MRCI value computed in the SV(P) basis at the TZVP- and TZVPP-optimized nuclear structures. We therefore conclude that it is advantageous to employ the same basis set for geometries and excitation energies.

Proceeding finally to adiabatic excitation energies (Table 3), few data are available for comparison. For the reasons discussed above, an optimized minimum geometry of the $2\,^1A_g$ state is not easily obtained. In the absence of the appropriate nuclear arrangement, we noticed that the absolute energy of the $2\,^1A_g$ takes the lowest value at the T_1 ($1\,^3B_u$) minimum geometry which is conceivable on the basis of qualitative arguments along the line of Walsh rules. For the $1\,^3B_u$ and $1\,^1B_u$ states, the UDFT- and TDDFT-optimized nuclear arrangements were employed, respectively. We find that the geometry relaxation effect on the excitation energy is much more pronounced for the $2\,^1A_g$ state than for the $1\,^1B_u$ state. Even at the relaxed $1\,^1B_u$ minimum geometry, we find the $2\,^1A_g$ state to lie more than 0.5 eV below the $1\,^1B_u$ state. This explains the seemingly conflicting obvervations by Buma et al.[44] and Petek et al.[45] on the one side and by Fujii et al.[64] on the other side and makes broad band widths of the hexatriene absorption spectrum[42] plausible. It appears that the two states are near degenerate in the FC region with the $2\,^1A_g$ state possibly located slightly above the optically bright $1\,^1B_u$ state. Upon geometry relaxation, the $2\,^1A_g$ state clearly becomes the S_1 state, opening a fast relaxation channel for the primarily occupied $1\,^1B_u$ state. Following the general trends, the DFT/MRCI calculations underestimate the adiabatic excitation energies of both states by about 0.2−0.3 eV. For the T_1 state we did not find a published value of the 0−0 energy, but we expect the deviation to be slightly smaller than in the singlet cases.

Octatetraene. In order to assess the results of the present theoretical study on OT, a short review of the experimental findings will be given first. Gas phase OT has been reported

Table 4. C−C Bond Distances [pm] in the Electronic Ground State of OT

	B-LYP[a]	B3-LYP[a]	BH-LYP[a]	HF[a]	MP2[a]	CASSCF[b]	exp[c]
C_4-C_3	136.1	134.8	133.4	132.9	135.1	134.5	133.6
C_3-C_2	145.3	145.0	144.9	146.4	145.1	145.7	145.1
C_2-C_1	137.5	136.0	134.3	133.5	136.1	135.1	132.7
$C_1-C_{1'}$	144.4	144.3	144.4	146.0	144.5	145.1	145.1

[a] Present work. SV(P) basis. [b] See ref 14. CASSCF with 8 active electrons in 12 active orbitals, (3s2p1d/2s) basis. [c] See ref 68. X-ray structure of crystalline OT.

to fluoresce from its S_2 ($1\,^1B_u$) state with a quantum yield of about 0.1.[40] The origin of the $1\,^1B_u \leftarrow 1\,^1A_g$ transition of jet-cooled OT is observed at 4.41 eV.[41,43] Since it represents the strongest peak in the absorption spectrum of OT, this value is frequently used also by theoreticians as a measure for the vertical excitation energy at the ground-state equilibrium geometry.[12,14,17] For lack of an alternative, we will do the same here, but we regard the comparison with some reservation. As detailed by Davidson and Jarzecki,[67] a comparison of the computed vertical excitation energy with the corresponding maximum in the absorption spectrum implicitly makes the assumption that the geometry displacement of the excited state is fairly large so that its vibrational wave function has maximal amplitude in the region of the classical turning points, which is not the case here. Gavin et al.[40] estimate the energy gap between the $1\,^1B_u$ and $2\,^1A_g$ state of OT to be approximately 0.8 eV, in line with the results of newer measurements. In 1999, Pfanstiel et al.[47] succeeded in recording a rotationally resolved one-photon fluorescence excitation spectrum of OT. The first strong band at 3.60 eV is located only marginally above the origin of the $2\,^1A_g \leftarrow 1\,^1A_g$ emission at 3.59 eV. In the condensed phase at 77 K, relaxed emission from the lower-lying $2\,^1A_g$ state of OT is observed with a quantum yield of approximately 0.6.[40] The origin transition of $2\,^1A_g \leftarrow 1\,^1A_g$ was determined by TPA in two different solvents.[54] The solvent shift of this transition is rather small. In contrast, the $1\,^1B_u$ state experiences large stabilization effects by the surrounding *n*-alkanes, decreasing the energy gap between the $1\,^1B_u$ and $2\,^1A_g$ state in *n*-hexane to approximately half of the gas phase value. This should be kept in mind when comparing quantum chemical results for isolated molecules with experimental data in the condensed phase.

Detailed information on the vertical and adiabatic excitation energies of the two lowest triplet states is available through electron energy loss spectra which were recorded with resolution of the vibrational structure by Allan et al.[51] The authors also observed the $1\,^1B_u \leftarrow 1\,^1A_g$ transition and a higher-lying band with origin and maximum at 6.04 eV which they tentatively assigned to the $2\,^1B_u \leftarrow 1\,^1A_g$ transition, but state that it could be due to the $3\,^1A_g$ state.

The results of the present theoretical investigation on OT are collected in Tables 4−6. The minimum nuclear arrangement of the electronic ground state was optimized using three different density functionals as well as HF and MP2. The resulting C−C bond lengths are displayed in Table 4 together with earlier theoretical values obtained at the CASSCF level[14] and crystal structure data.[68] It must be stressed again that in all cases the MO basis and the Fock matrix elements

Table 5. Dependence of DFT/MRCI Vertical Absorption ΔE_{vert} and Adiabatic Excitation Energies ΔE_{adia} [eV] of OT on the Geometry Parameters

	ΔE_{vert}, SV(P) basis							ΔE_{adia}, SV(P) basis			
geometry	B-LYP	B3-LYP	BH-LYP	HF	MP2	exp[a]	λ_{max}	B-LYP	B3-LYP	BH-LYP	ΔE_{0-0}
$2\,^1A_g$	3.82	4.02	4.26	4.48	4.01	4.41	≈4.1[b]	3.21[c]	3.25[c]	3.29[c]	3.59[d], 3.54[e], 3.56[f]
$1\,^1B_u$	4.24	4.33	4.45	4.57	4.33	4.54	4.40[g]	4.12	4.10	4.07	4.41[h], 4.41[i], 4.40[g]
$2\,^1B_u$	5.08	5.28	5.53	5.69	5.27	5.67					
$3\,^1A_g$	5.81	6.00	6.22	6.32	5.98	6.30					
$1\,^3B_u$	1.90	2.02	2.17	2.33	2.02	2.30	2.10[g]	1.53	1.53	1.51	1.73[g]
$1\,^3A_g$	3.21	3.32	3.44	3.50	3.30	3.46	3.55[g]				3.25[g]
$2\,^3B_u$	4.31	4.42	4.54	4.57	4.41	4.57					
$2\,^3A_g$	5.04	5.15	5.26	5.27	5.13	5.34					
$3\,^3B_u$	5.30	5.40	5.80	5.87	5.48	5.80					

[a] C−C bond distances adjusted to experimental values taken from ref 68. Crystal structure. [b] See ref 46. Estimated as 0−0 energy + 0.5 eV. [c] Energy at the $1\,^3B_u$ minimum. [d] See ref 47. Fluorescence excitation of jet-cooled OT. [e] See ref 54. Two-photon absorption in *n*-octane. [f] See ref 54. Two-photon absorption in *n*-hexane. [g] See ref 51. Electron energy loss of gaseous HT. [h] See ref 41. Absorption of jet-cooled OT. [i] See ref 43. Absorption and emission of jet-cooled OT.

Table 6. Basis Set Dependence of Calculated Vertical Absorption Energies ΔE_{vert} [eV] of OT and Comparison with Previous Theoretical Results of Correlated ab initio Wave Function Methods and Experimental Values

	DFT/MRCI			QCI/CI8[a]	CASPT2[b,c,d]			CC2[d]	CCSD[d]	CC3[d]	
state	SV(P)	TZVP	TZVPP								λ_{max}
$2\,^1A_g$	4.02	4.06	4.08	5.21	4.38	4.72	4.64	5.87	5.99	4.97	≈4.1[e]
$1\,^1B_u$	4.33	4.27	4.24	4.79	4.42	4.81	4.70	4.71	5.07	4.94	4.41[f], 4.41[g], 4.40[h]
$2\,^1B_u$	5.28	5.27	5.29			5.76	5.74	6.91	6.89	6.06	
$3\,^1A_g$	6.00	5.82	5.85			6.40	6.19	6.72	6.98	6.50	
$1\,^3B_u$	2.02	2.05	2.06	2.52	2.17	2.37	2.33	2.40	2.23	2.30	2.10[h]
$1\,^3A_g$	3.32	3.31	3.36		3.39	3.61	3.70	3.76	3.62	3.67	3.55[h]
$2\,^3B_u$	4.42	4.39	4.42			4.71					
$2\,^3A_g$	5.15	5.02	5.05			5.43					
$3\,^3B_u$	5.40	5.48	5.51								

[a] See ref 58. QCI for $2\,^1A_g$, CI8 + SC for $1\,^1B_u$ and $1\,^3B_u$. [b] See ref 13. CASPT2 based on CASSCF with 8 active electrons in 6 a_u and 5 b_g active orbitals, (4s3p1d/2s1p) ANO basis + Rydberg functions, experimental geometry parameters. [c] See ref 14. CASPT2 based on CASSCF with 8 active electrons in 12 active orbitals, (3s2p1d/2s) basis, experimental geometry parameters. [d] See ref 17. CASPT2 based on CASSCF with 8 active electrons in 8 active orbitals, TZVP basis, ground-state MP2/6-31G* geometry. [e] See ref 46. Estimated as 0−0 energy + 0.5 eV. [f] See ref 41 absorption of jet-cooled OT. [g] See ref 43. Absorption and emission of jet-cooled OT. [h] See ref 51. Electron energy loss of gaseous HT.

of the DFT/MRCI-Hamiltonian are constructed from a Kohn−Sham calculation employing the BH-LYP functional.

The performance of the B-LYP functional is interesting under cost considerations since the possibility to employ the RI approximation brings about an enormous speed-up of the geometry optimization compared to the hybrid functionals. The C−C bond length alternation of the B-LYP ground-state structure (no HF exchange) is less pronounced than in the B3-LYP minimum geometry (20% HF exchange) whereas the contrary is true for the BH-LYP functional (50% HF exchange). Comparing with the pure HF results it appears that a higher percentage of HF exchange leads primarily to a shortening of the double bonds while the single bond length variation is less pronounced. Addition of electron correlation, on the other hand, causes a decrease of the bond length alternation. The MP2- and B3-LYP-optimized geometries are nearly indistinguishable. These C−C bond lengths also closely resemble the CASSCF values published by Nakayama et al.[14] The X-ray values for the C−C single bond lengths[68] are comparable to the theoretical values. However, as already noticed by Serrano-Andrés et al.[12] and Nakayama et al.,[14] the X-ray value for the double bond adjacent to the central single bond in crystalline OT (132.7 pm)[68] is presumably too short.

For the study of the geometry dependence of vertical and adiabatic excitation energies (Table 5), we employed the SV(P) basis throughout. A less pronounced bond length alternation introduces a bias in favor of the excited states. Accordingly, the vertical DFT/MRCI excitation energies, computed at the B-LYP geometry, are consistently lower than at the B3-LYP geometry by about 0.2 eV for doubly excited states and about 0.1 eV for single excitations. Again the reverse trend is observed at the BH-LYP geometry and is continued for the HF geometry. The vertical DFT/MRCI excitation energies at the BH-LYP geometry are in good agreement with the experimental data, with the above-mentioned reservation that the position of the origin of the $1\,^1B_u \leftarrow 1\,^1A_g$ transition is not a good measure for the vertical excitation energy even if this is the strongest band in the vibrationally resolved spectrum. It might be worth noting in this context that in the parametrization of the DFT/MRCI-Hamiltonian against experimental band maxima originally BH-LYP optimized ground-state geometries were employed.[21] The general trend of the DFT/MRCI method to underestimate the true excitation energy might therefore partially result from a geometry effect during the parametrization. The decision, not to use the BH-LYP functional for geometry optimization is made on the basis of two facts: (1) The B3-LYP optimized geometry yields the lowest

Table 7. Calculated Vertical Absorption Energies ΔE_{vert} and Adiabatic Excitation Energies ΔE_{adia} [eV] of DP in Comparison with Previous Theoretical Results of Correlated ab initio Wave Function Methods and Experimental Values

	ΔE_{vert} (DFT/MRCI)			CASPT2[a]	ΔE_{adia} (DFT/MRCI)		
state	SV(P)	TZVP	TZVPP		SV(P)	TZVP	ΔE_{0-0}
$2\ ^1A_g$	3.40	3.44	3.46	3.95	2.68[b]	2.71[b]	3.07[c], 3.05[d], 3.10[e]
$1\ ^1B_u$	3.82	3.77	3.74	3.97	3.61	3.54	3.57[f,g], 3.98[e], 4.02[h]
$2\ ^1B_u$	4.55	4.57	4.59	4.91			
$3\ ^1A_g$	5.38	5.32	5.31	5.64			
$1\ ^3B_u$	1.73	1.76	1.77	1.95	1.28	1.37	
$1\ ^3A_g$	2.82	2.82	2.84	3.02			
$2\ ^3B_u$	3.85	3.83	3.86	4.07			
$2\ ^3A_g$	4.65	4.59	4.63	4.86			
$3\ ^3B_u$	4.69	4.70	4.73	4.97			

[a] See ref 14. CASPT2 based on CASSCF with 10 active electrons in 10 active orbitals, (3s2p1d/2s) basis, and experimental geometry parameters. [b] Energy at the $1\ ^3B_u$ minimum. [c] See ref 92. Two-photon absorption in *n*-heptane at 77 K. [d] See ref 92. Two-photon absorption in *n*-decane at 77 K. [e] See ref 69. 0−0 band measured in various solvents, corrected for solvent shifts. [f] See ref 92. Absorption and emission in *n*-heptane at 77 K. [g] See ref 92. Absorption and emission in *n*-decane at 77 K. [h] See ref 69. Origin of gas phase absorption.

absolute DFT/MRCI energy of the electronic ground state. (2) TDDFT calculations on the lowest triplet of longer polyenes are prone to triplet instabilities when the BH-LYP functional is employed. Interestingly, the influence of the particular choice of density functional for the geometry optimization levels off in case of the adiabatic DFT/MRCI excitation energies. Obviously, a partial cancelation of geometry effects occurs here.

Fortunately, the sensitivity of the DFT/MRCI energies with respect to the basis set (Table 6) is much less pronounced than the geometry dependence discussed above. As already seen for the polyacenes, an SV(P) basis appears to be sufficient. The DFT/MRCI method yields the correct order of low-lying singlet states. Admittedly, the 4.1 eV referred to as vertical excitation energy of the $2\ ^1A_g$ state by McDiarmid[46] is only a rough estimate. On the other hand, we know that the 0−0 energy of the $1\ ^1B_u \leftarrow 1\ ^1A_g$ transition is definitely a lower limit of the true vertical excitation energy. It is therefore clear that the $2\ ^1A_g$ state is located below the $1\ ^1B_u$ state in the FC region or that they are at most near degenerate. From the ab initio methods only the CASPT2 finds the $2\ ^1A_g$ state as the S_1 state. The CC3 method, which was employed by Schreiber et al.[17] for benchmark reasons only and is too expensive to be used in practical applications on large polyenes, obtains near degeneracy of the $1\ ^1B_u$ and $2\ ^1A_g$ states whereas the less demanding CC2 approach places the $2\ ^1A_g$ more than 1.1 eV above the $1\ ^1B_u$ state. Similarly large energy gaps with the wrong ordering of states are found for (TD)DFT treatments using hybrid functionals.[4]

Decapentaene. For *all-trans*-1,3,5,7,9-decapentaene, less experimental data are available. Vibrationally resolved fluorescence and one-photon excitation as well as TPA have been recorded in glassy *n*-alkanes.[55] A reliable estimate of the S_1 and S_2 origins was presented by D'Amico et al.[69] The formula which they employed for the extrapolation, $\nu(\text{solvent}) = \nu(\text{gas}) - k(n^2 - 1)/(n^2 + 2)$ where k is a fitting parameter and n is the refractive index of the solvent, yielded results in good agreement with gas phase data in the case of OT and the S_2 state of DP.

The DFT/MRCI results obtained for different AO bases (Table 7) are consistent with the findings in HT and OT. The vertical excitation energies are systematically lower than the CASPT2 results by Nakayama et al.,[14] but trends are well reproduced. A comparison with experiment can be made only for the adiabatic transitions between the ground state and the two lowest singlet excited states. The estimated S_1 and S_2 energies of isolated DP are underestimated by about 0.4 eV in this case, but the energy gap is in the right ballpark.

3.1.3. α, ω-Diphenyl-Polyenes. Similar trends are found for the short α, ω-diphenyl-polyenes, 1,6-diphenyl-*trans*, *trans*-1,3,5-hexatriene (DPHT), 1,8-diphenyl-*all-trans*-1,3,5,7-octatetraene (DPOT), 1,10-diphenyl-*all-trans*-1,3,5,7,9-decapentaene (DPDP), and 1,12-diphenyl-*all-trans*-1,3,5,7,9,11-dodecahexaene (DPDH). At first sight (Table 8), one might think that the deviations from the experimental excitation energies of the $1\ ^1B_u \leftarrow 1\ ^1A_g$ transition are smaller. However, for these molecules, only spectra in the condensed phase have been measured[7,70−74] and solvent effects are known to preferentially stabilize the $1\ ^1B_u$ state. In CS_2, a highly polarizable agent, even an inversion of the $1\ ^1B_u$ and $2\ ^1A_g$ levels has been observed.[73]

With regard to the cost of calculations on carotenoids, we investigated the basis set dependence and the sensitivity with respect to the density functional used for the geometry optimization. The same trends as for the short linear polyenes are found: The changes are very small when proceeding from the TZVPP basis over the TZVP basis to the SV(P) basis, whereas red shifts of the order of 0.1−0.2 eV are observed when the B-LYP geometry is employed instead of the B3-LYP geometry of the ground state. Detailed results are provided in Table 2 of the SI.

3.2. Longer Polyenes. From our benchmark results on shorter polyenes, α, ω-diphenyl-polyenes, and polyacenes and from recent results of the Thiel group,[17] we expect the DFT/MRCI energies at the B3-LYP optimized geometries to systematically underestimate the true energies of the electronically excited states. We did, however, not observe a bias toward one or the other type of state. It can therefore be expected that the energy gaps between the electronically excited states are reproduced well. Information on the performance of the DFT/MRCI method with respect to CPU time and on the number of CSFs included in the final MRCI space is available in the SI.

Table 8. DFT/MRCI Vertical Excitation Energies ΔE_{vert} and Adiabatic Excitation Energies ΔE_{adia} [eV] of α, ω-Diphenyl-polyenes in Comparison with Experimental Band Origins[a]

molecules	ΔE_{vert} (DFT/MRCI) SV(P)	ΔE_{vert} (DFT/MRCI) TZVP	ΔE_{adia} (DFT/MRCI) SV(P)	ΔE_{adia} (DFT/MRCI) TZVP	ΔE_{0-0}
			2 ^1A_g state[b]		
DPHT	3.47	3.51	2.86	2.87	3.19[c], 3.12[d]
DPOT	3.00	3.05	2.42	2.44	2.80[e], 2.77[d,f]
DPDP	2.64	2.70	2.08	2.11	2.50[g]
DPDH	2.35	2.42	1.84	1.84	2.26[g]
			1 ^1B_u state		
DPHT	3.36 (2.21)	3.34 (2.18)	3.15	3.10	3.62[c], 3.22[d], 3.23[d]
DPOT	3.08 (2.66)	3.07 (2.65)	2.88	2.85	3.01[e], 2.96[d], 3.02[f]
DPDP	2.85 (3.08)	2.85 (3.09)	2.66	2.64	2.86[g]
DPDH	2.66 (3.48)	2.67 (3.50)	2.47	2.46	2.72[g]
			1 ^3B_u state		
DPHT	1.78	1.81	1.38	1.39	1.50[h]
DPOT	1.56	1.59	1.17	1.19	
DPDP	1.39	1.43	1.02	1.04	
DPDH	1.25	1.29	0.89	0.91	

[a] Oscillator strengths for dipole-allowed transitions from the ground state are displayed in parentheses. [b] DFT/MRCI excitation energy at the 1 ^3B_u minimum. [c] See ref 73. Extrapolated vacuum origin. [d] See ref 71. Two-photon absorption at 77 K in EPA. [e] See ref 7. Emission spectrum recorded at 4.2 K in pentadecane. [f] See ref 70. Two-photon absorption at 77 K in EPA. [g] See ref 72. Excitation (1 $^1A_g \rightarrow$ 1 ^1B_u) and fluorescence (2 $^1A_g \rightarrow$ 2 ^1A_g) spectra recorded at 4.2 K in *n*-decane (DPDP) or *n*-dodecane (DPDH). [h] See ref 74. Triplet excitation spectra of DPHT crystals at 20 K.

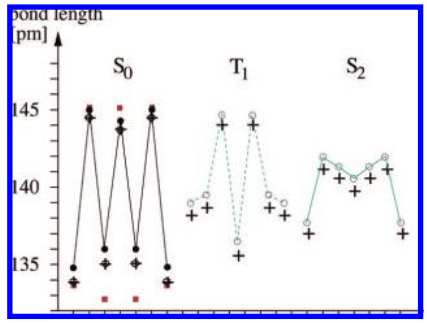

Figure 3. C−C bond lengths of *trans*,*trans*-1,3,5,7-octatetraene in the 1 ^1A_g electronic ground state (left), the first excited triplet state 1 ^3B_u (middle), and the optically bright 1 ^1B_u state (right). Calculated values are represented by circles (B3-LYP, SV(P) basis), plus signs (B3-LYP, TZVP basis), and hexagons (B3-LYP, TZVPP basis). Squares correspond to experimentally derived values determined from X-ray studies on crystalline OT.[68]

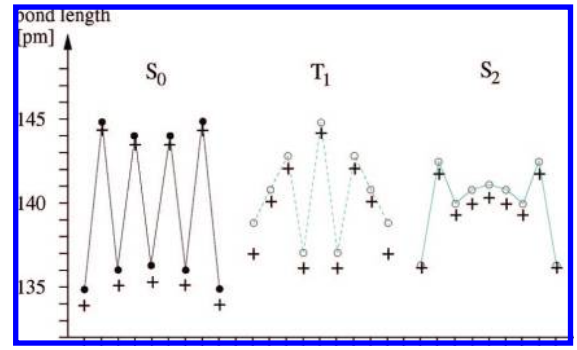

Figure 4. Calculated C−C bond lengths (circles: B3-LYP, SV(P) basis; plus signs: B3-LYP, TZVP basis) of *all-trans*-1,3,5,7,9-decapentaene in the 1 ^1A_g electronic ground state (left), the first excited triplet state 1 ^3B_u (middle), and the optically bright 1 ^1B_u state (right).

3.2.1. Vertical Excitation at the Ground State Geometry. The ground-state equilibrium structure is characterized by alternating double and single bonds wherein the bond length alternation is largest at the polyene ends and decreases slightly toward the center (Figure 5, top). The 1 ^3B_u state, which is dominated by the (HOMO → LUMO) single excitation, constitutes the lowest excited state in all polyenes. In the simple model of $2N$ independent electrons in a one-dimensional box of width L the excitation energy is given by the HOMO−LUMO orbital energy gap which is proportional to $(2N + 1)/L^2$. It is customary to assume that the box potential extends further than the distance between the first and last carbon atom which is approximately equal to $(2N - 1)$ times the average C−C bond length R_{CC}. Adding one bond length on either side of the polyene chain yields an estimate for the box width $L \propto (2N + 1)R_{CC}$. Within this model, a straight line would result if the vertical excitation energy is plotted as function of $1/(2N + 1)$. It is seen (Figure 6) that the excitation energies of the T_1 state nicely follow this simple scheme. The T_2 state, which comes next in the vertical excitation spectrum, possesses ^3A_g symmetry and has two leading configurations, (HOMO − 1 → LUMO) and (HOMO → LUMO + 1). With regard to its conjugation length dependence, a steeper slope and a larger deviation from linearity is observed in comparison to the T_1 state. This effect is even more pronounced for the corresponding singlet state, 2 ^1A_g. In addition to the above-mentioned (HOMO − 1 → LUMO) and (HOMO → LUMO + 1) single excitations, double excitations contribute to the CI expansion with high weight wherein the (HOMO → LUMO)^2 configuration is the leading term, in accord with earlier semiempirical calculations.[9,10] For the longer polyenes, also significant admixture with the double excitation (HOMO − 1, HOMO → LUMO, LUMO + 1) and the ground-state configuration is found. According to our calculations, this multiconfigurational expansion yields the lowest excited singlet state in all linear polyenes with $N \geq 3$, in agreement with experimental evidence.[7,8] Calculated vertical excitation energies of the S_1 state and the optically bright ^1B_u state, which results mainly from the (HOMO → LUMO) single excitation, can be found in Table 9. For all but the longest polyenes, the latter state is the second excited state at the ground-state

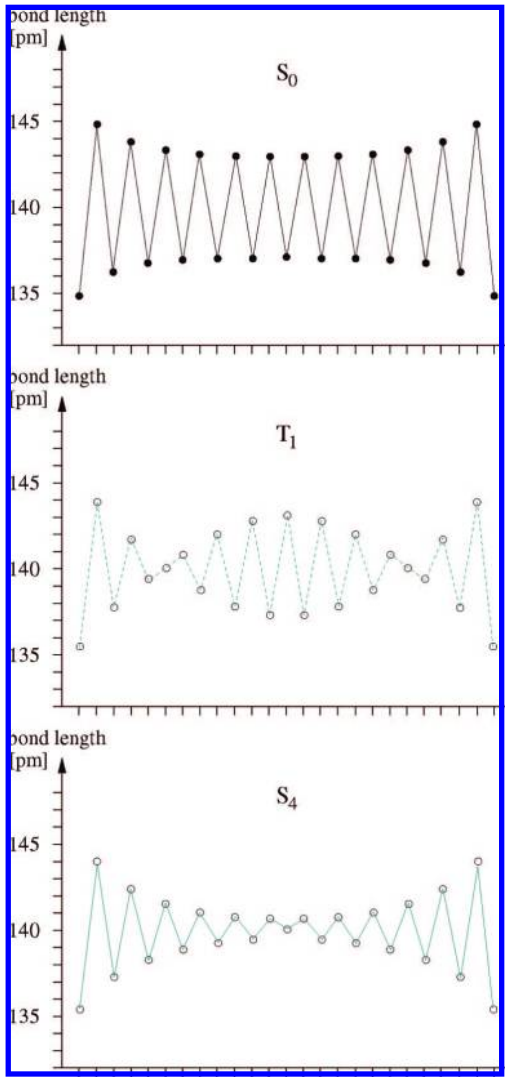

Figure 5. Calculated C−C bond lengths (B3-LYP, SV(P) basis) of *all-trans*-1,3,5,7,9,11,13,15,17,19,21,23,25-hexacosatridecaene in the 1 ^1A_g electronic ground state (top), the first excited triplet state 1 ^3B_u (middle), and the optically bright 1 ^1B_u state (bottom).

geometry. As discussed before, 1 ^1B_u is nearly degenerate with the 2 ^1A_g state and the 2 ^3B_u state in the vertical excitation spectrum of HT. The second singlet and triplet B_u states, symbolized by circles in Figure 6, and the third triplet B_u, symbolized by upside down triangles, have similarly strong multiconfigurational character as the 2 ^1A_g state. In the shorter polyenes the (HOMO − 2 → LUMO), (HOMO → LUMO + 2), and (HOMO − 1 → LUMO + 1) dominate these states while in the longer polyenes the doubly excited (HOMO − 1, HOMO → LUMO^2) and (HOMO^2 → LUMO, LUMO + 1) gain weight and become predominant in the 2 ^1B_u and 3 ^3B_u states. It is noteworthy that the order of the ^1B_u states changes with conjugation length. The optically bright ^1B_u state, frequently labeled $^1B_u^+$ in the literature wherein the + sign represents the so-called Pariser alternancy symmetry,[75] is the second excited state in the vertical excitation spectrum of short polyenes. According to our calculations, it becomes nearly degenerate with the second ^1B_u state, also denominated $^1B_u^-$ in the literature, for $N = 11$ while $^1B_u^+$ represents the third excited singlet

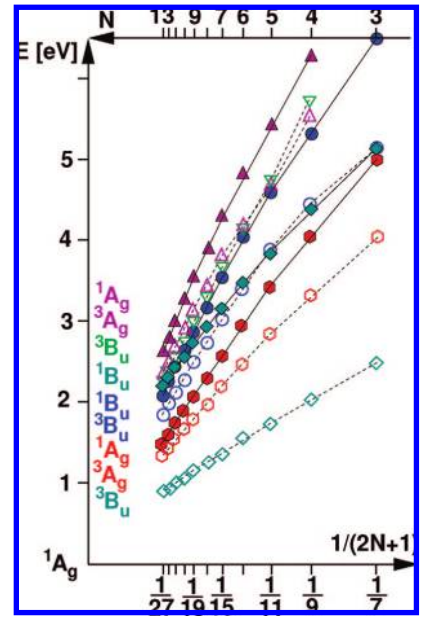

Figure 6. DFT/MRCI vertical electronic excitation energies of *all-trans*-polyenes at the respective 1 ^1A_g ground-state minimum geometry as functions of the conjugation length *N*. Filled symbols and solid lines correspond to singlet states, and open symbols and dashed lines, to triplet states. Squares, hexagons, and upside triangles symbolize A_g symmetric states; diamonds, circles, and upside down triangles symbolize B_u states.

state for longer polyenes. As we will see below, the location of the crossover is geometry dependent though. Let us finally turn to the 2 ^3A_g and 3 ^1A_g states which are the last ones that we have analyzed in detail. At the ground-state geometry, the 2 ^3A_g state is mainly composed of the single excitations (HOMO − 3 → LUMO), (HOMO − 2 → LUMO + 1), (HOMO → LUMO + 3), and (HOMO − 1 → LUMO + 2). The corresponding singlet, 3 ^1A_g, has significant contributions from the double excitations (HOMO − 2, HOMO → LUMO^2) and (HOMO^2 → LUMO, LUMO + 2) which become the leading terms in the longer polyenes.

3.2.2. Geometry Relaxation in the T_1 State. In the T_1 state, a reversal of single and double bond character is observed in the central parts of the polyenes (see Figures 2−4 for HT, OT, and DP, respectively, Figure 5 for *all-trans*-1,3,5,7,9,11,13,15,17,19,21,23,25-hexacosatridecaene (HCTD), and the SI for all other polyenes). The differences between alternating bond lengths become smaller when proceeding outward until subsequent bonds are nearly equal. This inner region comprises $N - 2$ bonds for odd N and $N - 1$ bonds for even N. Execpt for HT, which is too short to comply with this pattern, the inner region is followed by two (in the polyenes with even N) or three (in the polyenes with odd N) nearly equally long bonds. In the outer part, the bond alternation resembles the one in the ground state so that the terminal bond is always a short one, again except for the smallest members HT, OT, and DP.

This pattern was controversially discussed in the literature. Early studies by Kuki at al.[76] based on semiempirical Pariser−Parr−Pople single and double CI (SDCI) calculations observed strong bond alternation at the terminating carbon atoms and a loss of it in the central part of the polyene

Table 9. Vertical Absorption ΔE_{abs} and Emission ΔE_{em} Energies As Well As Adiabatic Excitation Energies ΔE_{adia} [eV] of Linear Polyenes with Conjugation Length N[a]

	$2\,^1A_g$			$1\,^1B_u/2\,^1B_u$[b]			$1\,^3B_u$		
N	ΔE_{abs}	ΔE_{em}[c]	ΔE_{adia}[c]	ΔE_{abs} ($f(r)$)	ΔE_{em} ($f(r)$)	ΔE_{adia}	ΔE_{abs}	ΔE_{em}	ΔE_{adia}
3	4.95	3.60	4.07	5.07 (1.39)	4.59 (1.33)	4.21	2.46	1.43	1.90
4	4.02	2.85	3.25	4.33 (1.82)	3.96 (1.77)	4.10	2.02	1.13	1.53
5	3.40	2.34	2.68	3.82 (2.24)	3.50 (2.20)	3.61	1.73	0.94	1.28
6	2.92	1.96	2.26	3.43 (2.64)	3.15 (2.60)	3.23	1.52	0.80	1.10
7	2.56	1.68	1.93	3.14 (3.02)	2.89 (2.98)	2.95	1.36	0.70	0.96
8	2.29	1.46	1.68	2.90 (3.40)	2.67 (3.15)	2.72	1.24	0.64	0.86
9	2.06	1.30	1.50	2.70 (3.76)	2.50 (3.72)	2.53	1.14	0.58	0.78
10	1.88	1.18	1.35	2.54 (4.11)	2.35 (4.08)	2.37	1.07	0.54	0.71
11	1.72	1.08	1.22	2.40 (4.30)	2.22 (4.44)	2.23	1.00	0.52	0.66
12	1.60	1.01	1.12	2.29 (4.78)	2.11 (4.79)	2.10	0.95	0.51	0.62
13	1.49	0.94	1.03	2.18 (5.10)	2.01 (5.14)	2.00	0.91	0.50	0.59

[a] Oscillator strengths $f(r)$ of symmetry-allowed vertical transitions are displayed in parentheses. [b] Ground state geometry: $1\,^1B_u$ for $N \leq 10$, $2\,^1B_u$ for $N \geq 11$; excited-state geometry $1\,^1B_u$ for $N \leq 7$, $2\,^1B_u$ for $N \geq 8$. [c] Relaxed geometry corresponds to the $1\,^3B_u$ minimum.

chain instead. The authors related this central domain of diminishing bond alternation to bond orders and postulated a "triplet-excited" region. Subsequent investigations by Takahasi et al.[77,78] pointed out the deficiencies in this approach: Their single-excitation CI (SCI) calculations on the series of polyenes from C_8H_{18} to $C_{22}H_{46}$ yielded geometries in agreement with Kuki et al. However, comparison calculations with CASSCF on octatetraene gave a considerably different bond alternation pattern which is consistent with our present calculations. Takahashi et al. concluded the appearance of the postulated "triplet-excited region" to be artifactual in SCI and SDCI calculations, related to the use of RHF MOs in combination with limitations on the excitations in the CI space. Consideration of the higher polyenes employing this method was not feasible, however. Geometry optimizations by Ma et al.[79,80] focusing on an assessment of the semiempirical Pariser−Parr−Pople model as well as providing results obtained with the UB3LYP method observed a bond alternation pattern which was qualitatively consistent with our study.

Inspection of the T_1 geometry pattern poses the question of a possible electron localization in the two regions of diminishing bond length. While Kuki et al. related their (erroneously established) domain of diminishing bond alternation to bond orders, Takahashi et al. as well as Ma et al. refrained from further conclusions in this respect in their later work, confining themselves to an observation of geometrical effects. Current work in our group concerning this particular question is underway.

The geometry relaxation effect on the excitation energies (Figure 7) is quite dramatic for some of the states as may be expected for a bond-order reversal in the central part of the chromophore. For the short polyenes, the energy gain in the $1\,^3B_u$ state is of the order of 0.5 eV and drops to 0.32 eV in HCTD. Calculated vertical and adiabatic excitation energies of the T_1 states of all polyenes are presented in Table 9. While the destabilization of the ground-state energy is rather strong for the short members, the effect levels off for the long polyenes. States which exhibit large expansion coefficients for configurations with doubly occupied LUMO ($2\,^1A_g$, $^1B_u^-$, $3\,^1A_g$, $3\,^3B_u$) experience huge stabilization effects. Qualitatively this can be understood from the fact that the electron density in the LUMO is large for those bonds which

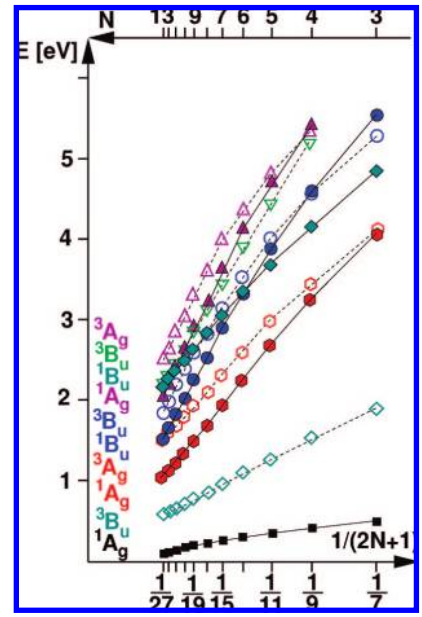

Figure 7. DFT/MRCI vertical electronic excitation energies of *all-trans*-polyenes at the first excited triplet $1\,^3B_u$ (HOMO → LUMO) minimum geometry as functions of the conjugation length N. The DFT/MRCI energy of the respective $1\,^1A_g$ ground-state minimum has been chosen as energy offset. For an explanation of symbols, see Figure 6.

correspond to short bonds in the T_1 state—at least in the central part of the chromophore. This stabilization of $(\mathrm{LUMO})^2$ occupations leads, for example, to the strange situation that the $2\,^1A_g$ state drops below the $1\,^3A_g$ state. Actually, the latter is slightly shifted to higher energies at the T_1 geometry. A further effect of the pronounced stabilization of the $^1B_u^-$ state is the significantly earlier crossover with the optically bright $^1B_u^+$ state which occurs already for $N = 6$ at the relaxed T_1 geometry. Inspite of its (HOMO → LUMO) character, the latter state is only slightly affected by the geometry relaxation in its triplet coupled counterpart. The reason for this behavior will become clear in the next section. Finally, for the longest polyenes ($N > 11$) we observe even a drop down of the $3\,^1A_g$ state below the $^1B_u^+$ state. Although it will be more meaningful to check the order of states at the relaxed $^1B_u^+$ geometry (see following section),

it is interesting to notice that a conical intersection between the two states occurs not far from the $^1B_u^+$ minimum.

3.2.3. Geometry Relaxation in the $^1B_u^+$ State. Although both the T_1 and the $^1B_u^+$ states are dominated by the (HOMO → LUMO) single excitation, relaxation of the nuclear coordinates leads to quite different equilibrium structures. We saw above that single and double bonds localize in the T_1 state in three different regions, i.e., the central and the two terminal parts of the polyene. These regions are separated by short sequences of C−C bonds where the bond alternation changes. In the $^1B_u^+$ state, double bond character is found for the terminal bonds, too, but in the central part of the polyene, bond lengths are nearly equalized (Figure 5). This bond length equalization is actually what one might have expected from a simple Walsh-type analysis of this electronic excitation. According to Walsh, the geometric parameters of a molecule correlate with the trends for the frontier orbital energies upon nuclear distortion.[81] The $(N - 1)$ nodes of the HOMO are placed where the LUMO exhibits maximal amplitudes and vice versa. In the $^{1,3}B_u^+$ states, the HOMO and LUMO are singly occupied each and single and double bond character should thus level out.

The energy gain of the $^1B_u^+$ state upon geometry relaxation to the minimum is of the order of 0.3 eV in the short polyenes and about 0.2 eV in the long ones (Table 9). The energies of the $^1B_u^+$ states at the respective T_1 geometries are only slightly less favorable. Together these facts indicate that the $^1B_u^+$ potential energy hypersurfaces (PEHs) of the longer polyenes are rather flat with respect to synchronous, but antiphase distortions of neighboring C−C bond lengths. We note in passing that a similar observation is made for the electronic ground states of the long polyenes which mix in non-negligible amounts of (HOMO → LUMO)^2 character. Their absolute DFT/MRCI energies are nearly identical at the S_0 and $^1B_u^+$ minimum geometries. The data in Table 9 show that the difference between the adiabatic excitation energies of the $2\ ^1A_g^-$ and $^1B_u^+$ state increases with the conjugation length and becomes nearly constant for the longer polyenes. Experimental energy differences that were corrected for solvent effects, have been published for octatetraene (0.791 eV), decapentaene (0.874 eV), and dodecahexaene (0.920 eV).[69] Our corresponding calculated values of 0.85, 0.93, and 0.97 eV are in the right ballpark and reflect the experimental trends. Also the calculated energy gap for $N = 11,\ 12,\ 13$ (roughly 1 eV) is in good agreement with the estimated long-chain limit of 7168 cm^{-1} (0.89 eV).[82]

Since there is no reversal of single- and double-bond character in the $^1B_u^+$ state, the energies of states that are characterized by a doubly occupied LUMO are less dramatically affected by the geometry relaxation than at the T_1 geometry. The stabilization of the $^1B_u^-$ state is sufficient, however, to cause a crossover between $N = 8$ and $N = 9$ where both states are near-degenerate. This near-degeneracy of states should manifest itself in perturbations in the spectra of these polyenes. It has to be noted, however, that the position of the intersection may vary with the solvent polarizability since the $^1B_u^+$ state is known to exhibit strong solvatochromic shifts. Actually, indications of such a near-degeneracy have been observed recently in femtosecond-resolved spectra of lutein, a pigment with 10 conjugated double bonds.[83] For carotenes with conjugation lengths $N \geq 9$, the presence of the $^1B_u^-$ state intermediate between $2^1A_g^-$ and $^1B_u^+$ has been postulated by several authors to assign resonance-Raman spectra or to explain the intricate relaxation dynamics of these compounds in femtosecond spectroscopy.[84−90]

3.2.4. Excited State Absorption. The longer polyenes show strong ESA and are thus interesting candidates for optical limiting. Triplet ESA will not be discussed here (although it is strong) because the triplet quantum yields of polyenes are known to be very small.

The excitation energies and oscillator strengths originating from the S_1 ($2\ ^1A_g$) state are collected in Table 10 for both the ground-state and the relaxed excited-state geometries. The strong geometry dependence of the transition energy and intensity of the first ESA band ($2\ ^1A_g \rightarrow 1\ ^1B_u$ in short polyenes, $2\ ^1A_g \rightarrow 2\ ^1B_u$ in the longer ones) is noteworthy. In particular for the long polyenes the use of the Franck−Condon approximation for the modeling of this ESA band appears questionable. The calculated ESA wavelengths of the longer polyenes are slightly smaller than half the laser wavelengths required for the $1\ ^1A_g \rightarrow 2\ ^1A_g$ TPA, even if the systematic errors of the DFT/MRCI $2\ ^1A_g$ excitation energies are taken into account. However, the energetic location of the upper $^1B_u^+$ state could be tuned into resonance by an appropriate choice of environment.

The very strong ESA in the visible and UVA range is due to (LUMO → LUMO + 1) excitations from S_1 to a higher, multiconfigurational ^1B_u state. In HT and OT, these excitations are spread over two valence ^1B_u states, but for the longer members of the series, the intensity is concentrated in a single transition. The numbering of the upper states may change upon geometry variation. At the relaxed S_1 geometry the upper state corresponds to $4\ ^1B_u$. While its transition frequency is less sensitive to geometry relaxation, we find a marked decrease of its oscillator strength. Energetically, it overlaps with the strong $1\ ^1A_g \rightarrow 1\ ^1B_u^+$ one-photon absorption and will thus be difficult to observe in experiments with low time resolution.

Some polyenes fluoresce from the $1\ ^1B_u^+$ (S_2/S_3) state. Therefore, ESA data have been computed for this state, too (Table 11). Huge oscillator strengths are found for an ESA transition in the visible to near-infrared spectral region. The upper ^1A_g state represents a (LUMO → LUMO + 1) excitation with respect to the $1\ ^1B_u^+$ state. It drifts from $4\ ^1A_g$ in HT to $6\ ^1A_g$ in the longer polyenes, but retains its electronic structure. A similar observation was recently made by Mikhailov et al.[91] who employed SAC-CI and an a posteriori TDA method in combination with the B3-LYP functional.

Although the oscillator strengths for $1\ ^1B_u^+ \rightarrow 6\ ^1A_g$ are larger than for the primary $1\ ^1A_g \rightarrow 1\ ^1B_u^+$ absorption, it will be difficult to reach a population inversion because the excitation energies do not match. Whether a tuning by solvent

Table 10. Singlet Excited State Absorption Bands ΔE_{ESA} [eV] of Linear Polyenes with Conjugation Length N[a]

	ΔE_{ESA} ($f(r)$)					
N	1 ^1B_u	2 ^1B_u	3 ^1B_u	4 ^1B_u	5 ^1B_u	6 ^1B_u
			2 ^1A_g state, FC region			
3	0.13	1.24	3.32 (0.16)	3.98 (0.65)	5.01 (0.01)	5.99
4	0.31 (0.01)	1.26	3.38 (0.74)	3.64 (0.56)	3.65	4.67 (0.01)
5	0.42 (0.01)	1.15	2.52	3.14 (1.64)	3.36 (0.12)	3.40
6	0.51 (0.02)	1.04	2.52	2.89 (2.13)	3.07 (0.03)	3.18 (0.01)
7	0.57 (0.03)	0.94	2.42	2.67 (2.51)	2.77 (0.03)	3.00
8	0.61 (0.04)	0.86	2.27	2.48 (2.60)	2.51 (0.31)	2.84
9	0.64 (0.05)	0.79	2.14	2.29 (0.03)	2.34 (3.25)	2.70
10	0.66 (0.07)	0.72	2.00	2.10	2.21(3.62)	2.57
11	0.67	0.68 (0.09)	1.87	1.93	2.09 (3.97)	2.46
12	0.62	0.69 (0.11)	1.75	1.80	2.00 (4.30)	2.36
13	0.58	0.69 (0.14)	1.65	1.68	1.91 (4.60)	2.27
	1 ^1B_u	2 ^1B_u	3 ^1B_u	4 ^1B_u	5 ^1B_u	6 ^1B_u
			2 ^1A_g state, relaxed[b]			
3	0.79(0.02)	1.46	3.97(0.30)	4.97(0.55)	5.38	6.62(0.01)
4	0.92(0.04)	1.33	3.83(0.97)	4.16(0.01)	4.58(0.37)	4.99
5	1.00(0.06)	1.20(0.01)	2.69	3.51(1.52)	3.96	4.26(0.24)
6	1.05(0.04)	1.09(0.06)	2.56	3.21(1.95)	3.60	4.00(0.18)
7	0.95	1.11(0.15)	2.43	2.97(2.29)	3.26	3.36
8	0.84	1.13(0.21)	2.25	2.75(2.56)	2.99	3.21
9	0.75	1.14(0.28)	2.08	2.56(2.82)	2.76	3.12
10	0.67	1.14(0.36)	1.92	2.41(3.02)	2.56	2.98
11	0.60	1.14(0.44)	1.77	2.28(3.17)	2.38	2.83
12	0.53	1.13(0.53)	1.64	2.16(3.31)	2.23	2.67
13	0.48	1.12(0.61)	1.52	2.06(3.41)	2.09(0.02)	2.52

[a] Oscillator strengths are displayed in parentheses. [b] DFT/MRCI excitation energies and oscillator strengths at the 1 ^3B_u minimum.

Table 11. Singlet Excited State Absorption Bands ΔE_{ESA} [eV] of Linear Polyenes with Conjugation Length N[a]

	ΔE_{ESA} ($f(r)$)			
N	3 ^1A_g	4 ^1A_g	5 ^1A_g	6 ^1A_g
	1 ^1B_u state for $N \leq 10$, 2 ^1B_u for $N \geq 11$, FC region			
3	2.09	2.94 (1.11)	3.12 (0.95)	4.86
4	1.67	1.82	2.45 (0.85)	2.64 (2.02)
5	1.56	1.60 (0.01)	2.02 (0.35)	2.30 (3.28)
6	1.36 (0.01)	1.42(0.01)	1.64 (0.13)	2.02 (4.22)
7	1.16 (0.01)	1.27 (0.02)	1.34 (0.07)	1.81 (4.96)
8	0.99 (0.01)	1.10 (0.06)	1.16	1.65 (5.66)
9	0.83	0.90 (0.05)	1.06	1.50 (6.31)
10	0.70	0.75(0.04)	0.98 (0.01)	1.39 (6.92)
11	0.59	0.63(0.04)	0.91 (0.01)	1.29 (7.26)
12	0.50	0.53(0.03)	0.85	1.21 (8.12)
13	0.42	0.44 (0.03)	0.79 (0.01)	1.14 (8.67)
	3 ^1A_g	4 ^1A_g	5 ^1A_g	6 ^1A_g
	1 ^1B_u state for $N \leq 7$, 2 ^1B_u for $N \geq 8$, relaxed			
3	2.23(0.01)	2.58(1.50)	2.91(0.47)	5.11
4	1.41(0.01)	1.93(0.03)	2.27(1.88)	2.44(0.89)
5	1.28(0.02)	1.69(0.04)	1.89(0.36)	2.06(3.16)
6	1.08(0.02)	1.51(0.06)	1.52(0.09)	1.82(4.13)
7	0.90(0.02)	1.23(0.04)	1.36(0.05)	1.63(4.86)
8	0.72(0.02)	1.00(0.02)	1.24(0.05)	1.48(5.25)
9	0.57(0.02)	0.81(0.01)	1.13(0.05)	1.35(6.22)
10	0.45(0.01)	0.66(0.01)	1.05(0.06)	1.24(6.84)
11	0.34(0.01)	0.53	0.97(0.05)	1.15(7.44)
12	0.26(0.01)	0.44	0.92(0.07)	1.08(8.01)
13	0.19(0.01)	0.35	0.86(0.05)	1.01(8.57)

[a] Oscillator strengths are displayed in parentheses.

effects is possible here cannot be concluded from the present data since the behavior of the upper state is not known.

Conclusions

The purpose of the present theoretical study was a critical assessment of the DFT/MRCI method in notoriously difficult cases where TDDFT in combination with standard functionals fails. In addition, the effects of various technical parameters of the calculations on the properties of the electronic states were thoroughly investigated.

The first of these cases is the position of the ^1L_a (HOMO−LUMO) transition in polyacenes. The DFT/MRCI energies follow the experimental trends with a tendency of slightly underestimating the true ^1L_a and ^1L_b excitation energies. Their accuracy is comparable to the one of the considerably more expensive ab initio CC2 method which overestimates the experimental values by approximately the same amount.

Static electron correlation in the multiconfigurational 2 ^1A_g state of linear polyenes and α,ω-diphenyl-polyenes is typically severely underrated by single-reference response methods such as TDDFT and CC2 with the result that the order of the 2 ^1A_g and 1 ^1B_u states is reversed in these calculations. The energy gap between these states is reproduced correctly by the DFT/MRCI method, but again the absolute excitation energies are somewhat too low. In linear polyenes with conjugation lengths 8 to 11 an interesting phenomenon is observed in the calculations. Upon geometry relaxation in the primarily excited $^1B_u^+$ state the multiconfigurational $^1B_u^-$ state is stabilized to an extent that an intersection between the corresponding potential energy hypersurfaces takes place. In polyenes with conjugation lengths 12 and 13, the $^1B_u^-$ state represents the S_2 state already in the Franck−Condon region. In the latter compounds, even the 3 ^1A_g drops down below the $^1B_u^+$ state. The presence of conical intersections between the optically bright $^1B_u^+$ state and dark singlet states lays the ground for the supposition that internal conversion after photoexcitation is extremely fast in the longer polyenes. Excited state absorption wave-

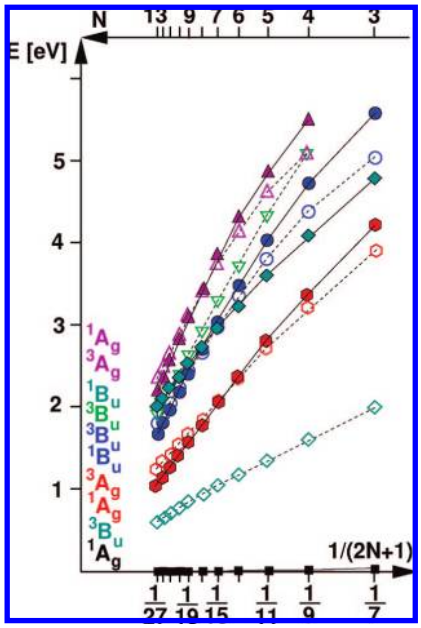

Figure 8. DFT/MRCI vertical electronic excitation energies of *all-trans*-polyenes at the minimum geometry of the optically bright ^1B_u (HOMO → LUMO) state as functions of the conjugation length *N*. The DFT/MRCI energy of the respective $1\ ^1A_g$ ground-state minimum has been chosen as energy offset. For an explanation of symbols, see Figure 6.

lengths and intensities are found to depend strongly on the nuclear geometry. In the gas phase, the wavelengths for ESA from the first excited singlet to the $^1B_u^+$ do not match with the laser wavelengths used for its two-photon excitation from the ground state. Due to its solvatochromism, the energetic location of the upper state could be tuned into resonance by an appropriate choice of environment, however.

With regard to the treatment of large π-systems it is encouraging that the reduction of the basis set quality from TZVPP over TZVP to SV(P) has almost no effect on the excitation energies and oscillator strengths. A more critical parameter is the ground-state equilibrium nuclear arrangement, at least in case of the polyene chains. As exemplified for *trans*,*trans*-1,3,5,7-octatetraene, where an experimental crystal structure is known, only the Hartree−Fock method yields C−C bond distances close to the experimental ones, most certainly due to a fortuitous error cancelation. All correlated methods applied (including the density functionals B-LYP, B3-LYP, and BH-LYP as well as the RIMP2, MP2, and CASSCF wave function approaches) underestimate the bond length alternation in the central part of the chromophore. These geometric deficiencies introduce a bias in favor of the electronically excited states of the polyenes, since the C−C bond length alternation is less pronounced or even reversed in the latter, offering an explanation for the fact that the DFT/MRCI electronic excitation energies of linear polyenes and α, ω-diphenyl-polyenes are consistently too low while the energy gaps between the excited states are reproduced well.

Acknowledgment. Intensive discussions with Alfred Holzwarth (MPI Mülheim) and Andreas Dreuw (Universität Frankfurt) during the progress of this work have been extremely valuable. Financial support from the Deutsche Forschungsgemeinschaft and the Heinrich-Heine-Universität Düsseldorf in the framework of the "Sonderforschungsbereich 663" is gratefully acknowledged.

Supporting Information Available: Tables S1 and S2 and Figures S1−S8. This material is available free of charge via the Internet at http://pubs.acs.org.

References

(1) Polivka, T.; Sundström, V. *Chem. Rev.* **2004**, *104*, 2021.

(2) Hsu, C.-P.; Hirata, S.; Head-Gordon, M. *J. Phys. Chem.* **2001**, *105*, 451.

(3) Wanko, M.; Garavelli, M.; Bernardi, F.; Niehaus, T. A.; Frauenheim, T.; Elstner, M. *J. Chem. Phys.* **2004**, *120*, 1674.

(4) Catalán, J.; de Paz, J. L. G. *J. Chem. Phys.* **2006**, *124*, 034306.

(5) Dreuw, A.; Head-Gordon, M. *Chem. Rev.* **2005**, *105*, 4009.

(6) Starcke, J. H.; Wormit, M.; Schirmer, J.; Dreuw, A. *Chem. Phys.* **2006**, *329*, 39.

(7) Hudson, B. S.; Kohler, B. E. *Chem. Phys. Lett.* **1972**, *14*, 299.

(8) Hudson, B. S.; Kohler, B. E. *J. Chem. Phys.* **1973**, *59*, 4984.

(9) Schulten, K.; Karplus, M. *Chem. Phys. Lett.* **1972**, *14*, 305.

(10) Tavan, P.; Schulten, K. *J. Chem. Phys.* **1979**, *70*, 5407.

(11) Tavan, P.; Schulten, K. *Phys. Rev. B* **1987**, *36*, 4337.

(12) Serrano-Andrés, A.; Lindh, R.; Roos, B. O.; Merchán, M. *J. Phys. Chem.* **193**, *97*, 9360.

(13) Serrano-Andrés, A.; Merchán, M.; Nebot-Gil, I.; Lindh, R.; Roos, B. O. *J. Chem. Phys.* **1993**, *98*, 3151.

(14) Nakayama, K.; Nakano, H.; Hirao, K. *Int. J. Quantum Chem.* **1998**, *66*, 157.

(15) Luo, Y.; Ågren, H.; Stafström, S. *J. Chem. Phys.* **1994**, *98*, 7782.

(16) Cronstrand, P.; Christiansen, O.; Norman, P.; Ågren, H. *Phys. Chem. Chem. Phys.* **2001**, *3*, 2567.

(17) Schreiber, M.; Silva-Junior, M. R.; Thiel, W.; Sauer, S. P. A. *J. Chem. Phys.* **2008**, *128*, 134110.

(18) Schirmer, J. *Phys. Rev. A* **1982**, *26*, 2395.

(19) Parac, M.; Grimme, S. *Chem. Phys.* **2003**, *292*, 11.

(20) Roos, B. O.; Andersson, K.; Fülscher, M. P. *Chem. Phys. Lett.* **1992**, *192*, 5.

(21) Grimme, S.; Waletzke, M. *J. Chem. Phys.* **1999**, *111*, 5645.

(22) Marian, C. M. *J. Chem. Phys.* **2005**, *122*, 104314.

(23) Kleinschmidt, M.; Tatchen, J.; Marian, C. M. *J. Chem. Phys.* **2006**, *124*, 124101.

(24) Tatchen, J.; Marian, C. M. *Phys. Chem. Chem. Phys.* **2006**, *8*, 2133.

(25) Marian, C. M. *J. Phys. Chem. A* **2007**, *111*, 1545.

(26) Perun, S.; Tatchen, J.; Marian, C. M. *ChemPhysChem* **2008**, *9*, 282.

(27) Salzmann, S.; Tatchen, J.; Marian, C. M. *J. Photochem. Photobiol. A: Chem.* **2008**, *198*, 221.

(28) Schäfer, A.; Huber, C.; Ahlrichs, R. *J. Chem. Phys.* **1994**, *100*, 5829.

(29) Furche, F.; Ahlrichs, R. *J. Chem. Phys.* **2002**, *117*, 7433.

(30) Ahlrichs, R.; et al. *TURBOMOLE*; version 5.6, Universität Karlsruhe, 2002.

(31) Becke, A. D. *Phys. Rev. A* **1988**, *38*, 3098.

(32) Lee, C.; Yang, W.; Parr, R. G. *Phys. Rev. B* **1988**, *37*, 785.

(33) Vahtras, O.; Almlöf, J.; Feyereisen, M. W. *Chem. Phys. Lett.* **1993**, *213*, 514.

(34) Eichkorn, K.; Treutler, O.; Öhm, H.; Häser, M.; Ahlrichs, R. *Chem. Phys. Lett.* **1995**, *240*, 283.

(35) Becke, A. D. *J. Chem. Phys.* **1993**, *98*, 5648.

(36) Stephens, P. J.; Devlin, F. J.; Chabalowski, C. F.; Frisch, M. J. *J. Phys. Chem.* **1994**, *98*, 11623.

(37) Becke, A. D. *J. Chem. Phys.* **1993**, *98*, 1372.

(38) Biermann, D.; Schmidt, W. *J. Am. Chem. Soc.* **1980**, *102*, 3163.

(39) Gavin, R. M., Jr.; Rice, S. A. *J. Chem. Phys.* **1974**, *60*, 3231.

(40) Gavin, R. M., Jr.; Weisman, C.; Rice, S. A. *J. Chem. Phys.* **1978**, *68*, 522.

(41) Leopold, D. G.; Vaida, V.; Granville, M. F. *J. Chem. Phys.* **1984**, *81*, 4210.

(42) Leopold, D. G.; Pendley, R. D.; Roebber, J. L.; Hemley, R. J.; Vaida, V. *J. Chem. Phys.* **1984**, *81*, 4218.

(43) Heimbrook, L. A.; Kohler, B. E.; Levy, I. J. *J. Chem. Phys.* **1984**, *81*, 1592.

(44) Buma, W. J.; Kohler, B. E.; Song, K. *J. Chem. Phys.* **1991**, *94*, 6367.

(45) Petek, H.; Bell, A. J.; Christensen, R. L.; Yoshihara, K. *J. Chem. Phys.* **1992**, *96*, 2412.

(46) McDiarmid, R. *Adv. Chem. Phys.* **1999**, *110*, 177.

(47) Pfanstiel, J. F.; Pratt, D. W.; Tounge, B. A.; Christensen, R. L. *J. Phys. Chem. A* **1999**, *103*, 2337.

(48) Post, D. E.; Hetherington, W. M., III; Hudson, B. *Chem. Phys. Lett.* **1975**, *35*, 259.

(49) Flicker, W. M.; Mosher, O. A.; Kuppermann, A. *Chem. Phys. Lett.* **1977**, *45*, 492.

(50) Frueholz, R. P.; Kuppermann, A. *J. Chem. Phys.* **1978**, *69*, 3433.

(51) Allan, M.; Neuhaus, L.; Haselbach, E. *Helv. Chim. Acta* **1984**, *67*, 1776.

(52) Trætteberg, M. *Acta Chem. Scand.* **1968**, *22*, 628.

(53) Granville, M. F.; Holtom, G. R.; Kohler, B. E. *J. Chem. Phys.* **1980**, *72*, 4671.

(54) Kohler, B. E.; Terpougov, V. *J. Chem. Phys.* **1996**, *104*, 9297.

(55) Kohler, B. E.; Terpougov, V. *J. Chem. Phys.* **1998**, *108*, 9586.

(56) Cave, R. J.; Davidson, E. R. *J. Phys. Chem.* **1988**, *92*, 614.

(57) Cave, R. J.; Davidson, E. R. *Chem. Phys. Lett.* **1988**, *148*, 190.

(58) Cave, R. J.; Davidson, E. R. *J. Phys. Chem.* **1988**, *92*, 2173.

(59) Li, X.; Paldus, J. *Int. J. Quantum Chem.* **1999**, *74*, 177.

(60) Woywod, C.; Livingood, W. C.; Frederick, J. H. *J. Chem. Phys.* **2000**, *112*, 613.

(61) Woywod, C. *Chem. Phys.* **2005**, *311*, 321.

(62) Petrenko, T.; Neese, F. *J. Chem. Phys.* **2007**, *127*, 164319.

(63) Cave, R. J.; Zhang, F.; Maitra, N. T.; Burke, K. *Chem. Phys. Lett.* **2004**, *389*, 39.

(64) Fujii, T.; Kamata, A.; Shimizu, M.; Adachi, Y.; Meada, S. *Chem. Phys. Lett.* **1985**, *115*, 369.

(65) Gavin, R. M., Jr.; Risenberg, S.; Rice, S. A. *J. Chem. Phys.* **1973**, *58*, 3160.

(66) Myers, A. B.; Pranata, K. S. *J. Phys. Chem.* **1989**, *93*, 5079.

(67) Davidson, E. R.; Jarzecki, A. A. *Chem. Phys. Lett.* **1998**, *285*, 155.

(68) Baughman, R. H.; Kohler, B. E.; Levy, I. J.; Spangler, C. *Synth. Met.* **1985**, *11*, 37.

(69) D'Amico, K. L.; Manos, C.; Christensen, F. L. *J. Am. Chem. Soc.* **1980**, *102*, 1777.

(70) Fang, H. L.-B.; Thrash, R. J.; Leroi, G. E. *J. Chem. Phys.* **1977**, *67*, 3389.

(71) Fang, H. L.-B.; Thrash, R. J.; Leroi, G. E. *Chem. Phys. Lett.* **1978**, *57*, 59.

(72) Horwitz, J. S.; Itoh, T.; Kohler, B. E.; Spangler, C. W. *J. Chem. Phys.* **1987**, *87*, 2433.

(73) Kohler, B. E.; Itoh, T. *J. Chem. Phys.* **1988**, *92*, 5120.

(74) Weiss, V.; Port, H.; Wolf, H. C. *Chem. Phys. Lett.* **1992**, *192*, 289.

(75) Pariser, R. *J. Chem. Phys.* **1956**, *24*, 324.

(76) Kuki, M.; Koyama, Y.; Nagae, H. *J. Phys. Chem.* **1991**, *95*, 7171.

(77) Takahashi, O.; Watanabe, M.; Kikuchi, O. *Theochem—J. Mol. Struct.* **1999**, *469*, 121.

(78) Takahashi, O.; Watanabe, M.; Kikuchi, O. *Int. J. Quantum Chem.* **1998**, *67*, 101.

(79) Ma, H.; Liu, C.; Jiang, Y. *J. Chem. Phys.* **2004**, *120*, 9316.

(80) Ma, H.; Cai, F.; Liu, C.; Jiang, Y. *J. Chem. Phys.* **2005**, *122*, 104909.

(81) Walsh, A. D. *J. Chem. Soc.* **1953**, 2260; 2266; 2288; 2296; 2301; 2306; 2318; 2321; 2325; 2330.

(82) Andersson, P. O.; Gillbro, T. *J. Chem. Phys.* **1995**, *103*, 2509.

(83) Holzwarth, A. L. in preparation, 2008.

(84) Sashima, T.; Koyama, Y.; Yamada, T.; Hashimoto, H. *J. Phys. Chem. B* **2000**, *104*, 5011.

(85) Yoshizawa, M.; Aoki, H.; Hashimoto, H. *Bull. Chem. Soc. Jpn.* **2002**, *75*, 949.

(86) Yoshizawa, M.; Aoki, H.; Hashimoto, H. *Phys. Rev. B* **2001**, *63*, 180301.

(87) Yoshizawa, M.; Aoki, H.; Ue, M.; Hashimoto, H. *Phys. Rev. B* **2003**, *67*, 174302.

(88) Larsen, D.; Papagiannakis, E.; I.H.M. van Stokkum, M. V.; Kennis, J.; van Grondelle, R. *Chem. Phys. Lett.* **2003**, *381*, 733.

(89) Polli, D.; Cerullo, G.; Lanzani, G.; Silvestri, S. D.; Yanagi, K.; Hashimoto, H.; Cogdell, R. *Phys. Rev. Lett.* **2004**, *93*, 163002.

(90) Kosumi, D.; Yanagi, K.; Nishio, T.; Hashimoto, H.; Yoshizawa, M. *Chem. Phys. Lett.* **2005**, *408*, 89.

(91) Mikhailov, I. A.; Tafur, S.; Masunov, A. E. *Phys. Rev. A* **2008**, *77*, 012510.

(92) Kohler, B. E.; Terpougov, V. *J. Chem. Phys.* **198**, *108*, 9586.

CT8001738